

OPEN

# Highly durable and flexible gallium-based oxide conductive-bridging random access memory

Kai-Jhih Gan<sup>1</sup>, Po-Tsun Liu<sup>2</sup>, Ta-Chun Chien<sup>2</sup>, Dun-Bao Ruan<sup>1</sup>  & Simon M. Sze<sup>1</sup>

The flexible conductive-bridging random access memory (CBRAM) device using a Cu/TiW/Ga<sub>2</sub>O<sub>3</sub>/Pt stack is fabricated on polyimide substrate with low thermal budget process. The CBRAM devices exhibit good memory-resistance characteristics, such as good memory window ( $>10^5$ ), low operation voltage, high endurance ( $>1.4 \times 10^2$  cycles), and large retention memory window ( $>10^5$ ). The temperature coefficient of resistance in the filament confirms that the conduction mechanism observed in the Ga<sub>2</sub>O<sub>3</sub> layer is similar with the phenomenon of electrochemical metallization (ECM). Moreover, the performance of CBRAM device will not be impacted during the flexibility test. Considering the excellent performance of the CBRAM device fabricated by low-temperature process, it may provide a promising potential for the applications of flexible integrated electronic circuits.

Flexible electronics are critical technologies for the development of wearable electronic equipment so that various electronic components, such as, organic light-emitting diodes (OLEDs), solar cells, sensors, and thin film transistors (TFTs), have been widely demonstrated on flexible substrates by many researchers<sup>1–9</sup>. Based on the trend, the demand for the flexible memory devices will also increase to assist the growth of flexible electronics. However, the conventional Flash memory is difficult to be integrated into flexible substrates due to the gate oxide quality degradation for the limited low-temperature process<sup>10,11</sup>. Notably, nonvolatile resistive random access memory (RRAM) was proposed and is the most promising candidate because of its simple structure, low temperature process, high scalability, and high packaging density<sup>12–14</sup>. A large amount of metal oxides have been studied for the RRAM applications<sup>15–18</sup>. Among of them, gallium oxide (Ga<sub>2</sub>O<sub>3</sub>) is well-known for its wide bandgap ( $E_g \sim 4.9$  eV), high dielectric constant, and compatible fabrication since it can be fabricated at room temperature<sup>19–21</sup>. In addition, gallium (Ga) is commonly used in the display industry to control the oxygen vacancy in the InGaZnO material due to its ease of combination with oxygen ions<sup>22</sup>. Therefore, Ga<sub>2</sub>O<sub>3</sub> can be considered as one of the promising candidates for RRAM devices. The widely recognized physical mechanism in RRAM devices can be divided into two categories, one is the oxide resistive random access memory (OxRRAM) and the other is the conductive-bridging random access memory (CBRAM)<sup>23,24</sup>. For the OxRRAM, the formation and rupture of the filaments is formed by oxygen vacancies within the RRAM device<sup>25–27</sup>. CBRAM is also referred to as electrochemical metallization (ECM) memory, relying on the formation/dissolution of metallic filaments inside the switching layer<sup>28–31</sup>. CBRAM shows larger memory window and more power usage effectiveness compared to the OxRAM<sup>32,33</sup>. The Cu-based CBRAM, which takes the advantage of the Cu line as the top electrode, is also a beneficial choice with respect to the reduction of RC propagation delay and cost-effective fabrication<sup>34,35</sup>. Flexible CBRAM will play an increasingly important role in flexible electronic systems, including data processing, information storage, and communication with external devices.

In this work, the device consisted of stacked Cu/TiW/Ga<sub>2</sub>O<sub>3</sub>/Pt structure is demonstrated on low-cost polyimide (PI) substrate processed at low temperature. Electrical characteristics of Ga<sub>2</sub>O<sub>3</sub> CBRAM devices are discussed in details, such as set/reset voltage, DC endurance property, and data retention. Good memory window with large high to low-resistance state (HRS/LRS) ratio of  $10^5$  can be achieved. In addition, the nature of conductive filament in the Ga<sub>2</sub>O<sub>3</sub> device is also explored. Highly durable Ga<sub>2</sub>O<sub>3</sub> CBRAM characteristics are exhibited in this work and provide a stage for the development of wearable electronic technology and large-area electronics.

<sup>1</sup>Department of Electronics Engineering, National Chiao Tung University, Hsinchu, 30010, Taiwan. <sup>2</sup>Department of Photonics and Institute of Electro-Optical Engineering, National Chiao Tung University, Hsinchu, 30010, Taiwan. Correspondence and requests for materials should be addressed to P.-T.L. (email: [ptliu@mail.nctu.edu.tw](mailto:ptliu@mail.nctu.edu.tw))

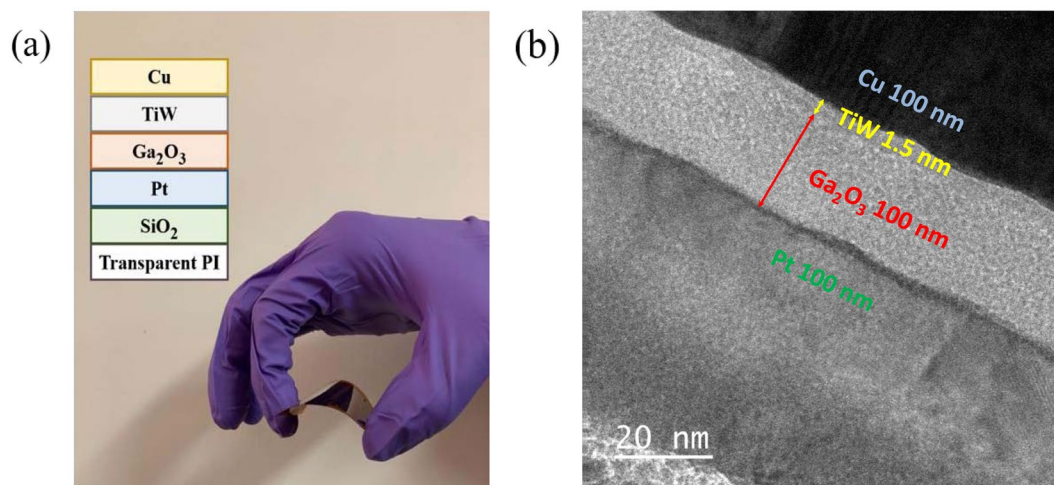


**Figure 1.** (a) Device photo of fabricated CBRAMs on flexible PI substrate. (b) Cross-sectional TEM image of the Cu/TiW/Ga<sub>2</sub>O<sub>3</sub>/Pt with 200 °C annealing in N<sub>2</sub> atmosphere.

## Results

Figure 1(a) shows the devices structure of Cu/TiW/Ga<sub>2</sub>O<sub>3</sub>/Pt CBRAM fabricated on flexible PI substrate. A TEM image of Ga<sub>2</sub>O<sub>3</sub> CBRAM device annealed at 200 °C in N<sub>2</sub> atmosphere clearly indicates that the thicknesses of the bottom electrode (Pt), switching layer (Ga<sub>2</sub>O<sub>3</sub>), barrier layer (TiW), and top electrode (Cu) layer are 100, 1.5, 20, and 100 nm, respectively.

For both forming and set processes, the current compliance of 100 μA is crucial to avoid a permanent or hard breakdown. The forming process was required to activate the CBRAM devices under DC sweeping mode. The forming voltage of the as-deposited Ga<sub>2</sub>O<sub>3</sub> CBRAM device was 5.9 V. However, the forming voltages of the device annealed at 200 °C in N<sub>2</sub> atmosphere is significantly decreased to 4.4 V. Figure 2(a,b) show the typical bipolar current-voltage (*I*-*V*) curves of the as-deposited CBRAM device and the device annealed at 200 °C on flexible PI, respectively. In the beginning, the low-resistance state (LRS) is achieved when conductive filaments in the Ga<sub>2</sub>O<sub>3</sub> switching layer are produced by Cu ion migration and stacking from the Cu to Pt bottom electrode in the Ga<sub>2</sub>O<sub>3</sub> layer; it's called the set process. Conversely, the high-resistance state (HRS) is achieved when conductive filaments in the switching layer are ruptured by Cu ion migration and stacking from the Pt to Cu electrodes in the Ga<sub>2</sub>O<sub>3</sub> layer; this is called the reset process. The DC endurance of the as-deposited device and the device annealed at 200 °C in N<sub>2</sub> atmosphere are depicted in Fig. 2(c,d), respectively. The performance of the as-deposited device is stable only up to 700 cycling endurance, while the device annealed at 200 °C in N<sub>2</sub> atmosphere exhibits the better endurance cycles over 1.4 × 10<sup>3</sup>. In order to investigate the uniformity of the switching parameters, the statistical variations in set voltage ( $V_{set}$ ) and reset voltage ( $V_{reset}$ ) for both devices were checked. Figure 2(e) indicates a substantial difference in the statistical distributions of  $V_{set}$  and  $V_{reset}$  between the devices. The coefficient of variation (CV) expresses the variation as a percentage of the mean, and is defined as the ratio of the standard deviation ( $\sigma$ ) to the mean value ( $\mu$ ). The distribution is improved from the as-deposited devices ( $CV_{set} = 33.8\%$ ,  $CV_{reset} = 58.8\%$ ) to the device annealed at 200 °C in N<sub>2</sub> atmosphere ( $CV_{set} = 29.1\%$ ,  $CV_{reset} = 57.8\%$ ). Moreover, the retention characteristics of our device are also studied, as shown in Fig. 2(f). For Ga<sub>2</sub>O<sub>3</sub> device annealed at 200 °C in N<sub>2</sub> atmosphere, HRS and LRS are quite stable, without significant resistance decay ( $HRS/LRS > 10^5$ ) even after 10<sup>4</sup> s operation at room temperature. According to the results mentioned above, the CBRAM annealed at 200 °C in N<sub>2</sub> atmosphere shows good performance and evinces its potential for the memory applications.

To further investigate the physical mechanism for the endurance improvement caused by the post-deposition annealing in N<sub>2</sub> atmosphere, material analysis was performed. The XPS spectra were performed with PHI Quantera SXM, using Al K $\alpha$  source (a beam power of 25 W and an emission current of 4.025 mA). The XPS spectrum of the O 1s signal was applied to examine the oxygen binding states at the surface of the Ga<sub>2</sub>O<sub>3</sub> thin film. The XPS result of the sample with Ga<sub>2</sub>O<sub>3</sub> switching layer without annealing process is shown in Fig. 3(a). The O 1s peak can be fitted by two nearly Gaussian distribution peaks, approximately located at 529.8 (FWHM = 1.6) and 531.1 eV (FWHM = 1.5), respectively. The lower binding energy peak located at 529.8 eV is attributed to oxygen-lattice bonds, which are related to the O<sup>2-</sup> ions combined with the Ga atoms in the Ga<sub>2</sub>O<sub>3</sub> compound system. On the other hand, the higher binding energy peak located at 531.1 eV can be attributed to oxygen-vacancy (O<sub>v</sub>) bonds. The O<sub>v</sub> peak is attributed to the oxygen deficient in the Ga<sub>2</sub>O<sub>3</sub> matrix. According to the XPS results shown in Fig. 3(a,b), it is important to notice that the proportion of oxygen-vacancy bonds (14.81%) of Ga<sub>2</sub>O<sub>3</sub> film annealed at 200 °C in N<sub>2</sub> atmosphere is higher than the one without annealing (7.17%). Therefore, the Ga<sub>2</sub>O<sub>3</sub> CBRAM devices at 200 °C in N<sub>2</sub> atmosphere exhibit good switching behaviors and lower  $V_{set}$  and  $V_{reset}$  caused by a considerable amount of oxygen vacancies in the oxide layer. This improvement can be attributed to these considerable oxygen vacancies which may lower the energy cost of Cu insertion into the Ga<sub>2</sub>O<sub>3</sub> layer, and lead to the Cu migration in the switching layer<sup>32</sup>.

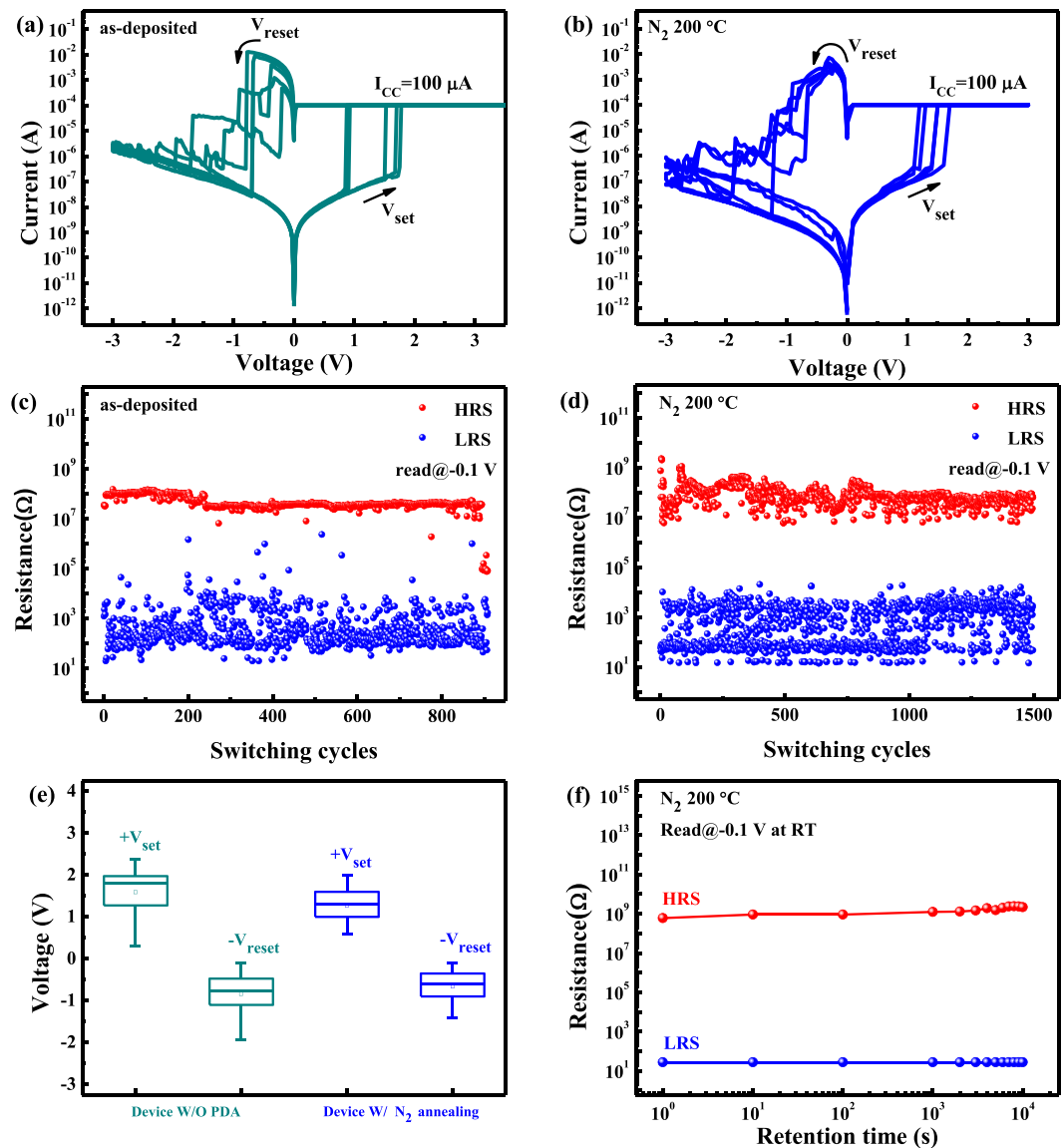


**Figure 2.** The typical bipolar I-V switching curves of (a)  $\text{Ga}_2\text{O}_3$  flexible CBRAM devices and (b)  $\text{Ga}_2\text{O}_3$  flexible CBRAM devices with 200 °C annealing in  $\text{N}_2$  atmosphere. The DC endurance characteristics of (c) as-deposited and (d) 200 °C  $\text{N}_2$  annealing  $\text{Ga}_2\text{O}_3$  flexible CBRAM devices (e) The statistical distribution of  $V_{\text{set}}$  and  $V_{\text{reset}}$  in the as-deposited and 200 °C  $\text{N}_2$  annealing  $\text{Ga}_2\text{O}_3$  flexible CBRAM devices. (f) Retention of 200 °C  $\text{N}_2$  annealing  $\text{Ga}_2\text{O}_3$  flexible CBRAM devices at room temperature.

In order to further understand the nature of conductive filaments, the conduction mechanism can be confirmed by the curve fitting. Firstly, we consider a linear temperature dependence of the conductive filament typical of metallic behavior, that is,  $R(T) = R(T_0) [1 + \gamma(T - T_0)]$ , where  $R(T)$  is the LRS resistance at temperature  $T$ ,  $R(T_0)$  is the LRS resistance at room temperature  $T_0$ , and  $\gamma$  is the temperature coefficients of resistance<sup>36,37</sup>. The LRS resistance of the devices is taken from 298 to 358 K and linearly increases with temperature, as shown in Fig. 4. For our devices, the temperature coefficients of resistance ( $\gamma$ ) is about  $8.77 \times 10^{-3} \text{ K}^{-1}$ . As shown in Table 1, the result is one order of magnitude more than that of oxygen vacancy assisted filaments ( $6.03 \times 10^{-4} \text{ K}^{-1}$ )<sup>38</sup>. The temperature coefficients obtained are close to the value  $1.3 \times 10^{-2} \text{ K}^{-1}$  for high-purity Cu assisted filaments<sup>39</sup>. Therefore, the formation and rupture of Cu-based conductive filaments is responsible for the resistive switching behavior in our devices.

Good mechanical flexibility is crucial for applications in flexible electronics. Then, the substrate is bent to different curvature radius of 5.0, 3.0, 1.0, and 0.5 cm with both tensile and compressive stresses. After each bending operation, the performance is evaluated by recording I-V curves on five different devices. As shown in Fig. 5(a,b), the  $R_{\text{LRS}}/R_{\text{HRS}}$  values are stable at more than  $10^5$  even after it is bent with different curvature radius. The statistical data in Fig. 5(c-f) may reveal that  $V_{\text{set}}$  and  $V_{\text{reset}}$  can be kept, almost the same with those of a fresh device. Furthermore, a continuous bending test of up to  $10^4$  times with curvature radius of 5.0 cm is carried out. Even at  $10^4$  bends, the  $R_{\text{LRS}}/R_{\text{HRS}}$  can be maintained, as shown in Fig. 5(g,h). These results indicate that a flexible  $\text{Ga}_2\text{O}_3$

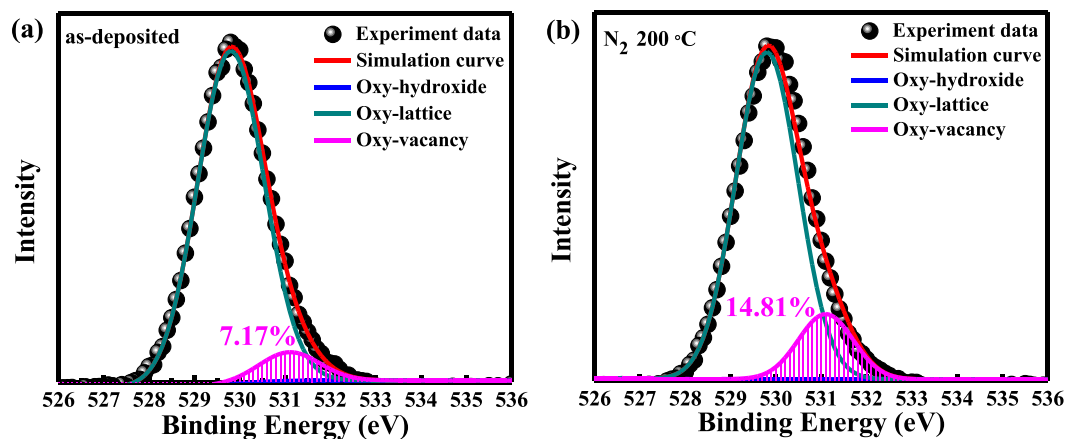


**Figure 3.** Analysis of the XPS O 1s spectrum on (a) the as-deposited Ga<sub>2</sub>O<sub>3</sub> thin film and (b) Ga<sub>2</sub>O<sub>3</sub> thin film annealed at 200 °C in N<sub>2</sub> atmosphere.

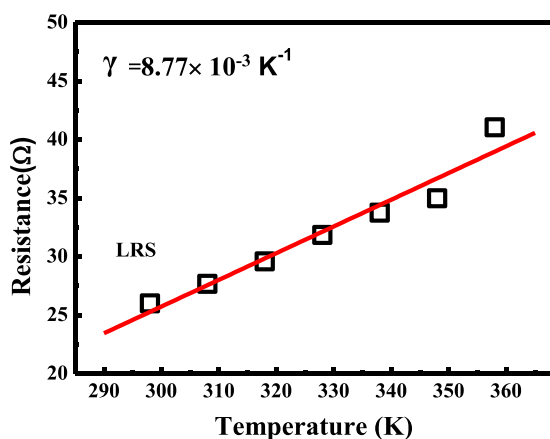


**Figure 4.** Temperature-dependent LRS resistance of Ga<sub>2</sub>O<sub>3</sub> CBRAM devices; the solid lines are the linear fit with an equation  $R(T) = R(T_0) [1 + \gamma(T - T_0)]$ .

RRAM	Cu/TiW/ ZrO <sub>2</sub> /TiN CBRAM <sup>39</sup>	Ga <sub>2</sub> O <sub>3</sub> CBRAM (this work)	Cu/Ta <sub>2</sub> O <sub>5</sub> / TiN CBRAM <sup>37</sup>	HfOx OxRRAM <sup>40</sup>	ZnO OxRRAM <sup>38</sup>
$\gamma(K^{-1})$	$1.3 \times 10^{-2}$	$8.77 \times 10^{-3}$	$3 \times 10^{-3}$	$8 \times 10^{-4}$	$6.03 \times 10^{-4}$
Types of conductive filament	Cu	Cu	Cu	Oxygen vacancy	Oxygen vacancy

**Table 1.** Comparison of the resistance temperature coefficient ( $\gamma$ ) of different RRAM devices.

CBRAM device with 200 °C annealing in N<sub>2</sub> atmosphere exhibits good flexibility, which suggests its possibility of commercially viable nonvolatile memory devices.

In summary, an amorphous Ga<sub>2</sub>O<sub>3</sub> CBRAM device annealed at 200 °C in N<sub>2</sub> atmosphere on low-cost flexible substrate is proposed for achieving good memory window, stable retention characteristics and a 2 times enhancement in endurance in this study. Through the current-voltage measurements, the device can be reliably operated in a low set voltage of 1.3 V and a low reset voltage of −0.65 V. The mechanism of the endurance enhancement effects is also ascribed to the generation of a considerable amount of oxygen vacancies in the Ga<sub>2</sub>O<sub>3</sub> layer by N<sub>2</sub> annealing, which may lead to the formation of Cu filaments. Analysis of the XPS O 1s depth distribution profile has been used to confirm this inference. Therefore, oxygen vacancies play a crucial role in resistive switching mechanism in Ga<sub>2</sub>O<sub>3</sub> CBRAM device. The extraction about the temperature dependence of resistance is an effectual method to examine the nature of the conductive filaments. The temperature coefficient of resistance is about  $8.77 \times 10^{-3} K^{-1}$  in this work, which means the devices are ECM-based RRAM with Cu filament. These results indicate that the flexible Ga<sub>2</sub>O<sub>3</sub> CBRAM is attractive for low-cost wearable devices and suitable for the future bendable displays.

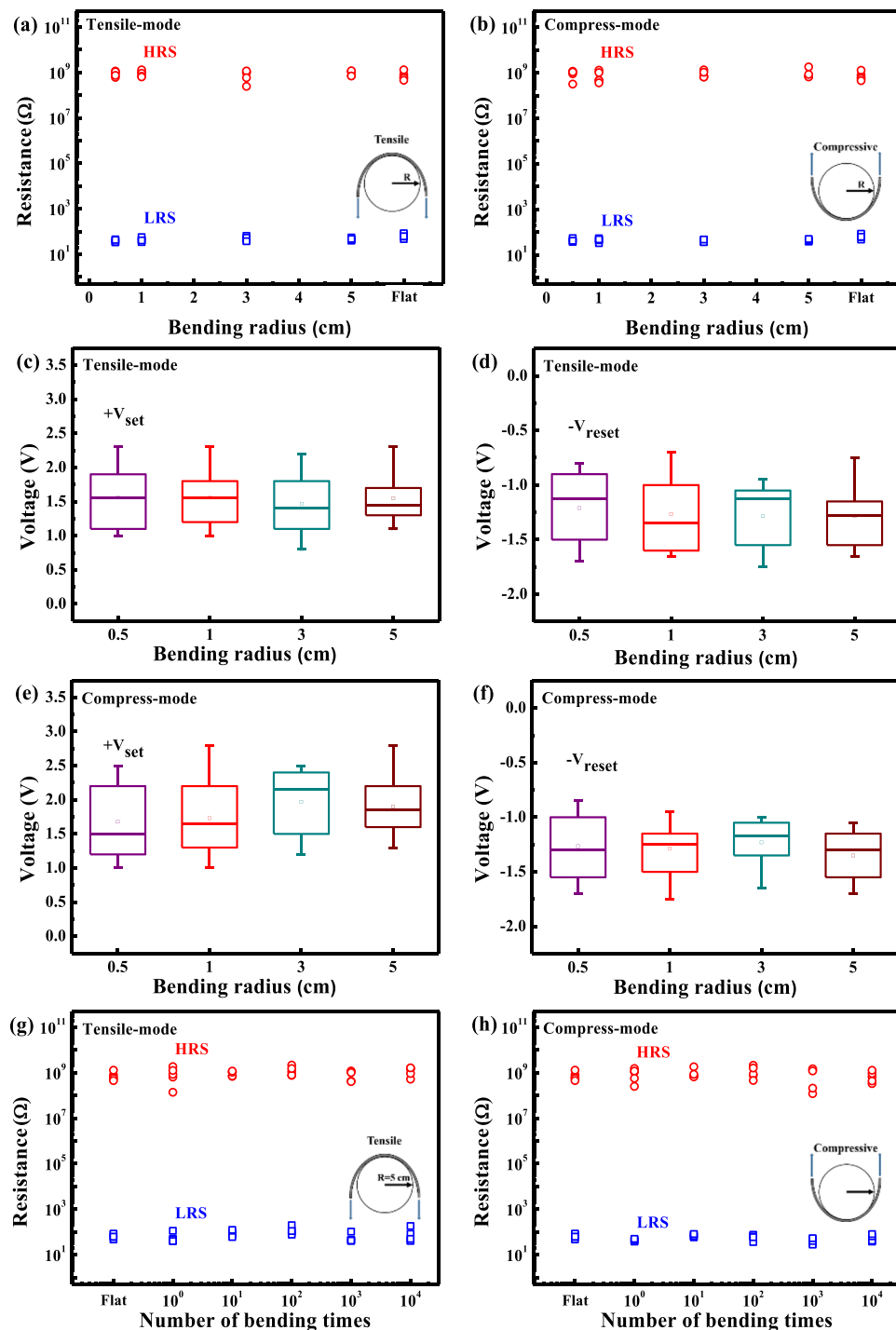


**Figure 5.** The values of LRS/HRS resistances after the device underwent different bending radius at (a) tensile test and (b) compressive test. (c,d) Statistical distributions of  $V_{set}$  and  $V_{reset}$  after the device underwent different bending radius at the tensile test. (e,f) Statistical distributions of  $V_{set}$  and  $V_{reset}$  after the device underwent different bending radius at the compressive test. Comparison of the current ratio between the LRS and HRS states of the flat and bent devices, along with the device after  $10^4$  continuous bending cycles at (g) tensile test and (h) compressive test. All data; five different devices were measured each time.

## Methods

The CBAM using Cu/TiW/Ga<sub>2</sub>O<sub>3</sub>/Pt stacks were successfully fabricated with limited process temperature of 200 °C on a flexible PI substrate. Firstly, the PI substrate was cleaned ultrasonically with ethanol for 5 mins and DI water. After cleaning up a PI substrate, a thin 100 nm SiO<sub>2</sub> buffer layer was deposited on PI substrate by plasma enhanced chemical vapor deposition. Then, 100 nm-thick Pt bottom electrode with 5 nm-thick Ti adhesion layer was deposited by using direct-current (DC) magnetron sputtering. Then, a 20 nm-thick Ga<sub>2</sub>O<sub>3</sub> film was deposited



on a Pt/Ti/SiO<sub>2</sub>/PI substrate by radio-frequency magnetron sputtering at room temperature. The deposition pressure was kept at 0.4 Pa, while the ratio of Ar:O<sub>2</sub> gas flow was kept at 1:1. The optimization of Ga<sub>2</sub>O<sub>3</sub> resistive switching layer deposition was applied in this work. Except for the control sample, a post-deposition annealing in N<sub>2</sub> atmosphere is applied at 200 °C for 30 mins. Finally, 1.5 nm-thick TiW barrier layer and 100 nm-thick Cu top electrodes were deposited by using DC magnetron sputtering and patterned with a shadow mask with a diameter of 100 μm. Electrical measurements were recorded by Keithley 4200 semiconductor characterization analyzer. To investigate the endurance improvement, transmission electron microscope (TEM) and X-ray photoelectron spectroscopy (XPS) were used to analyze the material properties.

## References

- Chen, Y. *et al.* Flexible active-matrix electronic ink display. *Nature* **423**, 136–136, <https://doi.org/10.1038/423136a> (2003).
- Docampo, P., Ball, J. M., Darwich, M., Eperon, G. E. & Snaith, H. J. Efficient organometal trihalide perovskite planar-heterojunction solar cells on flexible polymer substrates. *Nat. Commun.* **4**, 2761, <https://doi.org/10.1038/ncomms3761> (2013).
- Ju, S. *et al.* Fabrication of fully transparent nanowire transistors for transparent and flexible electronics. *Nat. Nanotechnol.* **2**, 378, <https://doi.org/10.1038/nnano.2007.151> (2007).
- Liu, P. T. *et al.* Highly Responsive Blue Light Sensor with Amorphous Indium-Zinc-Oxide Thin-Film Transistor based Architecture. *Scientific Reports* **8**, 8153, <https://doi.org/10.1038/s41598-018-26580-5> (2018).
- Ruan, D. B. *et al.* Photoresponsivity Enhancement and Extension of the Detection Spectrum for Amorphous Oxide Semiconductor Based Sensors. *Advanced Electronic Materials* **5**, <https://doi.org/10.1002/aelm.201800824> (2019).
- Ruan, D. B. *et al.* Investigation of low operation voltage InZnSnO thin-film transistors with different high-k gate dielectric by physical vapor deposition. *Thin Solid Films* **660**, 885–890, <https://doi.org/10.1016/j.tsf.2018.02.036> (2018).
- Ruan, D. B. *et al.* Mobility enhancement for high stability tungsten-doped indium-zinc oxide thin film transistors with a channel passivation layer. *Rsc Advances* **8**, 6925–6930, <https://doi.org/10.1039/c7ra13193c> (2018).
- Ruan, D. B. *et al.* Performance improvements of tungsten and zinc doped indium oxide thin film transistor by fluorine based double plasma treatment with a high-K gate dielectric. *Thin Solid Films* **665**, 117–122, <https://doi.org/10.1016/j.tsf.2018.07.053> (2018).
- Ruan, D. B. *et al.* The influence on electrical characteristics of amorphous indium tungsten oxide thin film transistors with multi-stacked active layer structure. *Thin Solid Films* **666**, 94–99, <https://doi.org/10.1016/j.tsf.2018.09.005> (2018).
- Woo, J. *et al.* Introduction of WO<sub>3</sub> Layer in a Cu-Based Al<sub>2</sub>O<sub>3</sub> Conductive Bridge RAM System for Robust Cycling and Large Memory Window. *IEEE J. of the Electron Devices Soc.* **4**, 163–166, <https://doi.org/10.1109/jeds.2016.2526632> (2016).
- Yang, F. M. *et al.* Nickel nanocrystals with HfO<sub>2</sub> blocking oxide for nonvolatile memory application. *Appl. Phys. Lett.* **90**, 222104, <https://doi.org/10.1063/1.2743926> (2007).
- Gan, K. J. *et al.* TAOS based Cu/TiW/IGZO/Ga<sub>2</sub>O<sub>3</sub>/Pt bilayer CBRAM for low-power display technology. *Surf. Coat. Technol.* **354**, 169–174, <https://doi.org/10.1016/j.surfcoat.2018.08.093> (2018).
- Hsu, C. H., Fan, Y. S. & Liu, P. T. Multilevel resistive switching memory with amorphous InGaZnO-based thin film. *Appl. Phys. Lett.* **102**, 062905, <https://doi.org/10.1063/1.4792316> (2013).
- Liu, P. T., Fan, Y. S. & Chen, C. C. Improvement of resistive switching uniformity for Al–Zn–Sn–O-based memory device with inserting HfO<sub>2</sub> layer. *IEEE Electron Device Lett.* **35**, 1233–1235, <https://doi.org/10.1109/LED.2014.2363491> (2014).
- Chang, K. C. *et al.* Dual ion effect of the lithium silicate resistance random access memory. *IEEE Electron Device Lett.* **35**, 530–532, <https://doi.org/10.1109/LED.2014.2311295> (2014).
- Hsu, C. W. & Chou, L. J. Bipolar Resistive Switching of Single Gold-in-Ga<sub>2</sub>O<sub>3</sub> Nanowire. *Nano Lett.* **12**, 4247–4253, <https://doi.org/10.1021/nl301855u> (2012).
- Sarkar, B., Lee, B. & Misra, V. Understanding the gradual reset in Pt/Al<sub>2</sub>O<sub>3</sub>/Ni RRAM for synaptic applications. *Semicond. Sci. Technol.* **30**, 105014, <https://doi.org/10.1088/0268-1242/30/10/105014> (2015).
- Tu, C. H. *et al.* Improved memory window for Ge nanocrystals embedded in SiON layer. *Appl. Phys. Lett.* **89**, 162105, <https://doi.org/10.1063/1.2362972> (2006).
- Choi, K. H. & Kang, H. C. Structural and optical evolution of Ga<sub>2</sub>O<sub>3</sub>/glass thin films deposited by radio frequency magnetron sputtering. *Mater. Lett.* **123**, 160–164, <https://doi.org/10.1016/j.matlet.2014.03.038> (2014).
- Marie, P., Portier, X. & Cardin, J. Growth and characterization of gallium oxide thin films by radiofrequency magnetron sputtering. *Phy. Status Solidi A* **205**, 1943–1946, <https://doi.org/10.1002/pssa.200778856> (2008).
- Stepanov, S. I., Nikolaev, V. I., Bougrov, V. E. & Romanov, A. E. Gallium oxide: Properties and applications - A review. *Rev. Adv. Mater. Sci.* **44**, 63–86 (2016).
- Ruan, D. B. *et al.* Effect of interfacial layer on device performance of metal oxide thin-film transistor with a multilayer high-k gate stack. *Thin Solid Films* **660**, 578–584, <https://doi.org/10.1016/j.tsf.2018.05.024> (2018).
- Gan, K. J. *et al.* Bipolar resistive switching characteristics of tungsten-doped indium-zinc oxide conductive-bridging random access memory. *Vacuum* **166**, 226–230, <https://doi.org/10.1016/j.vacuum.2019.05.023> (2019).
- Ye, C. *et al.* Physical Mechanism and Performance Factors of Metal Oxide Based Resistive Switching Memory: A Review. *Journal of Materials Science & Technology* **32**, 1–11, <https://doi.org/10.1016/j.jmst.2015.10.018> (2016).
- Fan, Y. S., Liu, P. T. & Hsu, C. H. Investigation on amorphous InGaZnO based resistive switching memory with low-power, high-speed, high reliability. *Thin Solid Films* **549**, 54–58, <https://doi.org/10.1016/j.tsf.2013.09.033> (2013).
- Shima, H., Takahashi, M., Naitoh, Y. & Akinaga, H. Electrode Material Dependence of Resistance Change Behavior in Ta<sub>2</sub>O<sub>5</sub> Resistive Analog Neuromorphic Device. *IEEE J. Electron Devices Soc.* **6**, 1220–1226, <https://doi.org/10.1109/JEDS.2018.2875942> (2018).
- Naitoh, Y. *et al.* Thermal robustness evaluation of nonvolatile memory using Pt nanogaps. *Appl. Phys. Express* **11**, 085202, <https://doi.org/10.7567/APEX.11.085202> (2018).
- Guy, J. *et al.* Experimental and theoretical understanding of Forming, SET and RESET operations in Conductive Bridge RAM (CBRAM) for memory stack optimization. *IEEE Int. Electron Devices Meet.*, 6.5.1, <https://doi.org/10.1109/IEDM.2014.7046997> (2014).
- Tsai, T. L., Jiang, F. S., Ho, C. H., Lin, C. H. & Tseng, T. Y. Enhanced Properties in Conductive-Bridge Resistive Switching Memory With Oxide-Nitride Bilayer Structure. *IEEE Electron Device Lett.* **37**, 1284–1287, <https://doi.org/10.1109/led.2016.2602886> (2016).
- Loy, D. J. J., Dananjaya, P. A., Hong, X. L., Shum, D. P. & Lew, W. S. Conduction Mechanisms on High Retention Annealed MgO-based Resistive Switching Memory Devices. *Scientific Reports* **8**, 14774, <https://doi.org/10.1038/s41598-018-33198-0> (2018).
- Hadi, S. A. *et al.* Bipolar Cu/HfO<sub>2</sub>/p<sup>++</sup> Si Memristors by Sol-Gel Spin Coating Method and Their Application to Environmental Sensing. *Scientific Reports* **9**, 9983, <https://doi.org/10.1038/s41598-019-46443-x> (2019).
- Piccolboni, G. *et al.* Vertical CBRAM (V-CBRAM): from experimental data to design perspectives. *2016 IEEE 8th International Memory Workshop*, <https://doi.org/10.1109/3DIC.2012.6263047> (2016).
- Tsai, T. L., Chang, H. Y., Jiang, F. S. & Tseng, T. Y. Impact of Post-Oxide Deposition Annealing on Resistive Switching in HfO<sub>2</sub>-Based Oxide RRAM and Conductive-Bridge RAM Devices. *IEEE Electron Device Lett.* **36**, 1146–1148, <https://doi.org/10.1109/led.2015.2477491> (2015).

34. Yu, S. *et al.* Design guidelines for 3D RRAM cross-point architecture. *2014 IEEE Int. Symposium on Circuit and Systems*, 421–424, <https://doi.org/10.1109/ISCAS.2014.6865155> (2014)
35. Belmonte, A. *et al.* A Thermally Stable and High-Performance 90-nm Al<sub>2</sub>O<sub>3</sub>/Cu-Based 1T1R CBRAM Cell. *IEEE Trans. Electron Devices* **60**, 3690–3695, <https://doi.org/10.1109/ted.2013.2282000> (2013).
36. Guan, W. H., Liu, M., Long, S. B., Liu, Q. & Wang, W. On the resistive switching mechanisms of Cu/ZrO<sub>2</sub>/Cu/Pt. *Appl. Phys. Lett.* **93**, <https://doi.org/10.1063/1.3039079> (2008).
37. Kang, Y. H., Liu, T., Potnis, T. & Orłowski, M. K. Composite Cu/V-O and V-O/Cu Nanofilaments in Cu/Ta<sub>2</sub>O<sub>5</sub>/Pt Devices. *Ecs Solid State Lett.* **2**, Q54–Q57, <https://doi.org/10.1149/2.004307ssl> (2013).
38. Wang, Z. Q. *et al.* Performance improvement of resistive switching memory achieved by enhancing local-electric-field near electromigrated Ag-nanoclusters. *Nanoscale* **5**, 4490–4494, <https://doi.org/10.1039/c3nr33692a> (2013).
39. Chandrasekaran, S., Simanjuntak, F. M., Aluguri, R. & Tseng, T. Y. The impact of TiW barrier layer thickness dependent transition from electro-chemical metallization memory to valence change memory in ZrO<sub>2</sub>-based resistive switching random access memory devices. *Thin Solid Films* **660**, 777–781, <https://doi.org/10.1016/j.tsf.2018.03.065> (2018).
40. Zhang, H. Z. & Ang, D. S. Zero temperature coefficient of resistance of the electrical breakdown path in ultrathin hafnia. *J. Phys. D* **50**, 385102, <https://doi.org/10.1088/1361-6463/aa7ec0> (2017).

## Acknowledgements

The authors would like to thank the National Chiao Tung University of Taiwan, and the Ministry of Science and Technology, Taiwan, R.O.C., for financially supporting this research under Contract: MOST 106-2221-E-009-107-MY3.

## Author Contributions

Prof. P.T. Liu and K.J. Gan wrote the main manuscript text. Prof. P.T. Liu designed experiments and directed the research direction including experimental and theoretical investigations for the devices. K.J. Gan and T.C. Chien fabricated the devices and measured the electrical characteristics of devices. D.B. Ruan contributed to the analysis of the XPS. Prof. Simon M. Sze reviewed the manuscript.

## Additional Information

**Competing Interests:** The authors declare no competing interests.

**Publisher's note** Springer Nature remains neutral with regard to jurisdictional claims in published maps and institutional affiliations.



**Open Access** This article is licensed under a Creative Commons Attribution 4.0 International License, which permits use, sharing, adaptation, distribution and reproduction in any medium or format, as long as you give appropriate credit to the original author(s) and the source, provide a link to the Creative Commons license, and indicate if changes were made. The images or other third party material in this article are included in the article's Creative Commons license, unless indicated otherwise in a credit line to the material. If material is not included in the article's Creative Commons license and your intended use is not permitted by statutory regulation or exceeds the permitted use, you will need to obtain permission directly from the copyright holder. To view a copy of this license, visit <http://creativecommons.org/licenses/by/4.0/>.

© The Author(s) 2019